BISON Fuel Performance Analysis of IFA-796 Rod 3 & 4 and Investigation of the Impact of Fuel Creep

Nuclear Technology Research and Development

Contents

LIST OF FIGURES

LIST OF TABLES

ACKNOWLEDGEMENTS

ABSTRACT

In order to improve the accident tolerance of light water reactor (LWR) fuel, alternative cladding materials have been proposed to replace the currently used zirconium (Zr)-based alloys. Of these materials, there is a particular focus on iron-chromium-aluminum (FeCrAl) alloys because they exhibit slower oxidation kinetics in high-temperature steam than Zr-alloys. This should decrease the energy release due to oxidation and slow cladding consumption in the presence of high temperature steam. These alloys should also exhibit increased "coping time" in the event of an accident scenario by improving the mechanical performance at high temperatures, allowing greater flexibility to achieve core cooling. As a continuation of the development of these alloys, in-reactor irradiation testing of FeCrAl cladded fuel rods has started. In order to provide insight on the possible behavior of these fuel rods as they undergo irradiation in the Halden Boiling Water Reactor, engineering analysis has been performed using FeCrAl material models implemented into the BISON fuel performance code.

This milestone report provides an update on the ongoing development of modeling capability to predict FeCrAl cladding fuel performance and to provide an early look at the possible behavior of planned in-reactor FeCrAl cladding experiments. In particular, this report consists of two separate analyses. The first analysis consists of fuel performance simulations of IFA-796 rod 4 and two segments of rod 3. These simulations utilize previously implemented material models for the C35M FeCrAl alloy and UO_2 to provide a bounding behavior analysis corresponding to variation of the initial fuel cladding gap thickness within the fuel rod. The second analysis is an assessment of the fuel and cladding stress states after modification of the fuel creep model that is currently implemented in the BISON fuel performance code.

Effects from modifying the fuel creep model were identified for the BISON simulations of the IFA-796 rod 4 experiment, but show that varying the creep model (within the range investigated here) only provide a minimal increase in the fuel radius and maximum cladding hoop stress. Continued investigation of fuel behavioral models will include benchmarking the modified fuel creep model against available experimental data, as well as an investigation of the role that fuel cracking will play in the compliance of the fuel. Correctly calculating stress evolution in the fuel is key to assessing fuel behavior up to gap closure and the subsequent deformation of the cladding due to PCMI. The inclusion of frictional contact should also be investigated to determine the axial elongation of the fuel rods for comparison with data from this experiment.

BISON FUEL PERFORMANCE ANALYSIS IFA-796 ROD 3 & 4

1. INTRODUCTION

During the accident progression in a light water reactor, such as a beyond design basis accident, the capacity to cool the fuel in the core may be lost. In such a scenario, the fuel and cladding temperatures quickly begin to increase, eventually reaching temperatures where the coolant begins to boil and evaporate. As this occurs, the coolant level in the core decreases, and the fuel can become uncovered. Without sufficient heat transfer from the fuel rods to the coolant, the temperature of the fuel and cladding will increase dramatically. In the case of traditional zirconium-based cladding materials, as the temperature of the cladding reaches ~1200˚C, the zirconium rapidly begins to oxidize with H_2O in the coolant and steam. This oxidation reaction causes both thinning of the Zr-alloy cladding as the metal oxidizes and releases large amounts of H_2 gas into the reactor pressure vessel [1]. With prolonged exposure, the cladding can rupture, releasing fission products into the coolant.

In order to increase the margin of safety for LWR fuel cladding in accident scenarios, several alternative materials have been proposed to replace the currently used zirconium-based cladding. Of these materials, there is a particular focus on select iron-chromium-aluminum (FeCrAl) alloys due to much slower oxidation kinetics in high-temperature steam than zirconium-based alloys [2]. This increased oxidation resistance may provide more time to mitigate any further damage resulting from an accident.

To continue the process of characterizing candidate accident tolerant fuel materials, irradiation testing, using an instrumented fuel assembly (IFA-796), has been scheduled in the Halden Boiling Water Reactor. The IFA-796 test is designed to irradiate six fuel rod positions, to be filled with a combination of fuel rods and fuel rod segments, consisting of various accident tolerant fuel cladding concepts. In order to support ongoing experimental characterization of FeCrAl cladding behavior, fuel performance simulations have been performed for relevant FeCrAl cladded fuel rods under anticipated reactor conditions.

This milestone report consists of two separate analyses. The first analysis consists of fuel performance simulations of IFA-796 rod 4 and two segments of rod 3. These simulations utilize previously implemented material models for the C35M FeCrAl alloy and UO_2 to provide a bounding behavior analysis corresponding to variation of the initial fuel cladding gap thickness within the fuel rod. The second analysis is an assessment of the fuel and cladding stress states after modification of the fuel creep model that is currently implemented in the BISON fuel performance code. This is performed to more accurately determine the mechanical response of the fuel and cladding after pellet-cladding mechanical interaction (PCMI) occurs.

2. MODELING APPROACH

We have used the BISON fuel performance code to simulate the FeCrAl cladded fuel rod and fuel rod segments in IFA-796 [3]. This fuel assembly is expected to contain three separate specimens with FeCrAl cladding. The first two specimens are segments of a fuel rod loaded at different axial positions in the Rod 3 location of the IFA-796 test rig. The third specimen is a full-size test rod spanning all four available segment locations in the Rod 4 location. A range of values for cladding thickness and fuel radius are assumed based on the measured variability of the cladding wall thickness across its periphery and the radius of the fuel pellets as manufactured. The values used for these simulations are organized to provide bounding behavior if the fuel rod was manufactured to have the largest possible gap thickness, the smallest possible gap thickness, and an average gap thickness. The fuel rod geometry specifications gathered from personal correspondence and an IFA-796 characterization report [4] are shown in Table 1.

Table 1. IFA-796 Fuel Rod Geometry

Simulation	Fuel Radius (µm)	Gap thickness (µm)	Cladding Thickness (µm)	Fuel Rod Outer Diameter (mm)	Fuel Stack Height (cm)	Cladding Length (cm)
Rod 4 - Max Gap	4335	65	371	9.542		
Rod 4 - Avg Gap	4338.5	54.5	381	9.548	50	60
Rod 4 - Min Gap	4342	44	391	9.554		
Rod 3 - Max Gap	4335	65	371	9.542		
Rod 3 - Avg Gap	4338.5	54.5	381	9.548	13.3	16
Rod 3 - Min Gap	4342	44	391	9.554		

To model the C36M3 FeCrAl cladding and UO_2 fuel, these simulations use several previously developed materials models currently implemented in BISON [5]. The cladding models used include: C35M Elastic modulus and poisons ratio [6], Kanthal APMT thermal expansion [7], C35M thermal creep [8], and irradiation creep and swelling [9]. Material properties used to simulate UO_2, including thermal and mechanical behavior models, fission gas release, fission product swelling, and fuel pellet relocation, are included in BISON and documented by Hales et al. [10]. These simulations use frictionless mechanical contact, which may influence the axial elongation of the cladding after mechanical contact has occurred.

The fuel rods are simulated under a constant linear heat rate of 20 kW/m, although the original linear heat rate target was nearly 25 kW/m, and use a flat axial power profile. This experiment targets a final fuel burnup of ~ 40 MWd/kgU, the fuel rods are simulated to a fuel average burnup of 60 MWd/kgU.

The IFA-796 irradiation rig is connected to a test loop designed to utilize prototypic PWR conditions. The reactor operating parameters are summarized in Table 2. A simple coolant temperature profile is applied along rod 4; the different sections of rod 3 use a temperature profile based on their axial location.

Table 2. IFA-796 fuel parameters and PWR loop conditions

Quantity	Value
Coolant Pressure	15.5 MPa
Coolant Temperature	Inlet: 568K Outlet: 593K
Initial Plenum Pressure	1 MPa
Fuel Density	95% T.D.
Average Fuel Grain Size	10 µm
UO_2 Fuel Enrichment	5%

2.1 UO_2 Creep Model

The UO_2 creep model included in BISON is a modified version of the FCREEP combined thermal and irradiation

creep model (eq. 1) described by Hagrman et al. [11]. FCREEP is assessed in order to identify sensitivity of the cladding stress state to uncertainties in the fuel compliance, specifically the contribution from fission-induced creep. This model is defined as the summation of the three separate creep contributions shown in eq. 1; fission-enhanced thermal creep (first term), thermal creep (second term), and fission-induced creep (third term).

$$\dot{\varepsilon}_{total} = \frac{A_1 + A_2 \dot{F}}{(A_3 + D) G^2} \sigma e^{\left(\frac{-Q_1}{RT}\right)} + \frac{A_4}{(A_6 + D)} \sigma^{4.5} e^{\left(\frac{-Q_2}{RT}\right)} + A_7 \dot{F} \sigma e^{\left(\frac{-Q_3}{RT}\right)} \tag{1}$$

Where the various A parameters, are fitting parameters, $\dot{F}$ is the fission rate (m^{-3}-s^{-1}), σ is the effective stress (Pa), the Q variables are creep activation energies (J-mol^{-1}), T is the temperature (K), R is the gas constant (J-K^{-1}-mol^{-1}), D is the percent of theoretical fuel density, and G is the grain size (μm). While there is an effect of the fuel stoichiometry on the creep activation energies (Q) for this model, only an oxide-to-metal ratio of 2 is considered. Values for the material constants are shown in table 3.

Table 3. Tabulated constants for the fuel creep [10-11] and modified fission-induced creep [12]

Parameter	Value	Units
A_1	0.3919	μm^2-Pa^{-1}-s^{-1}
A_2	1.31e-19	μm^2-m^3-Pa^{-1}
A_3	-87.7	*dimensionless*
A_4	2.0391e-25	Pa$^{-4.5}$-s^{-1}
A_6	-90.5	*dimensionless*
A_7	3.72264e-35	m^3-Pa^{-1}
A_8	1.49977e-36	m^3-Pa^{-1}
Q_1	4.5294e4	J/mol
Q_2	6.6432e4	J/mol
Q_3	2.6167e-3	J/mol

The fission-induced creep contribution is generally thought to be athermal [12], although there is some variability in reporting a temperature dependence [13]. This is especially important because the contribution from fission-induced creep dominates the total creep response approaching 1000˚C, where irradiation-enhanced creep becomes dominant.

In order to determine the differences from including athermal fission-induced creep in the creep rate calculation, the contribution in Eq. 1 was replaced by the athermal contribution from Solomon et al., shown in Equation 2. Figure 1 shows an example of the individual contributions in the combined thermal and irradiation creep model and eq. 2 for some common fuel parameters.

$$\dot{\varepsilon}_{3,b} = A_8 \dot{F} \sigma \tag{2}$$

Where the A parameter is a fitting parameter, $\dot{F}$ is the fission rate (m^{-3}-s^{-1}), and σ is the effective stress (Pa).
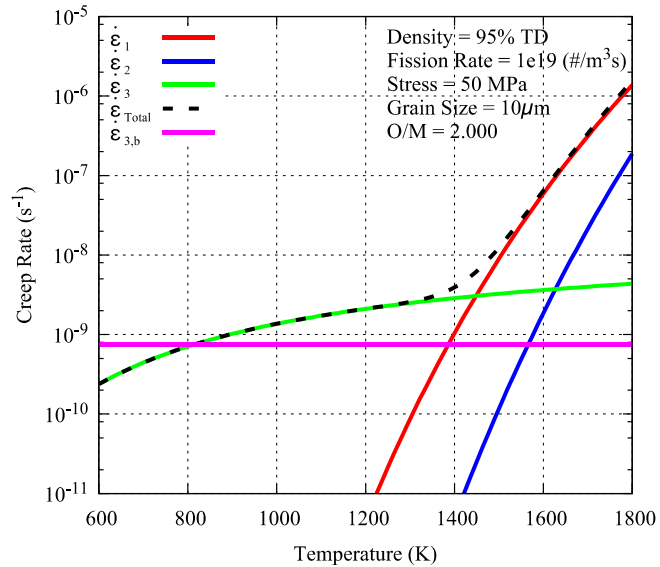
Figure 1. Plot of the individual contributions ($\dot{\varepsilon}_1, \dot{\varepsilon}_2, \dot{\varepsilon}_3$) to the total fuel creep rate ($\dot{\varepsilon}_{Total}$) in the model described by Hagrman [11] and a comparison with the athermal irradiation-induced fuel creep ($\dot{\varepsilon}_{3,b}$) contribution described by Solomon [12].

For the analysis described in Sections 3.1 and 3.2, the modified fuel creep model described in this section is used. Section 3.3 shows the effect that making this modification has on the cladding radial deformation and hoop stress after pellet-cladding contact has occurred. Because BISON does not currently track the size evolution of individual fuel grains during the simulations, a static value for the grain size is assumed for the entire fuel stack. Section 3.3 also contains a short evaluation of this assumption by dividing the fuel stack into radial zones and prescribing a different grain size to each zone.

3.   RESULTS AND DISCUSSION

The BISON fuel performance code was used to provide engineering analysis on the full-length rod 4 and the top-mid and bottom segments of rod 3 in the IFA-796 fuel assembly. The following results and discussion provide a systematic description of several relevant fuel rod performance indicators over the simulations including: the maximum fuel centerline temperature, cladding elongation, cladding radial deformation, maximum cladding hoop stress, fission gas release, and plenum pressure. Although the target discharge burnup for these test rods is 40 MWd/kgU, the BISON simulations of the fuel performance of these rods has been extended to 60 MWd/kgU to show possible fuel rod behavior if the target burnup is surpassed. It is once again pertinent to indicate that frictionless contact has been modeled for all cases within this report, and this will impact the predictions of axial deformation after the fuel – cladding gap has closed. The target burnup is displayed in these plots using a grey vertical line.

3.1 Rod 3 – Top-mid Section

The top-mid segment of rod 3 was simulated to 60 MWd/kgU. The peak fuel centerline temperature for all three fuel rod geometries over the fuel utilization is shown in Figure 2. As the fuel rod is initially heated, a difference among the simulations can be observed based on the fuel rod gap thickness. The fuel centerline temperatures continue to increase, even as the UO_2 thermal conductivity degrades, despite solid fission product swelling and fuel relocation increasing the fuel pellet diameter. As the gap closes, heat transfer between the fuel and cladding improves, working to slow the increase in fuel temperatures until gap closure occurs. The onset of gap closure for the *Minimum Gap* simulation begins at ~35 MWd/kgU where the edge of the smeared pellet fuel stack expands to locally contact the cladding. At ~40 MWd/kgU gap closure in the simulation is fully established with the rest of the fuel column in contact with the FeCrAl cladding. This occurs for the *Average Gap* and *Maximum Gap* simulations as well, with the onset of gap closure occurring at ~42 MWd/kgU and ~50 MWd/kgU and fully established mechanical contact occurring at ~46 MWd/kgU and ~55 MWd/kgU, respectively. Because the fuel temperatures in these simulations are low (< 1300K), they release very small amounts of gaseous fission products to the to the fuel rod plenum; the gap conductivity remains relatively unaffected.
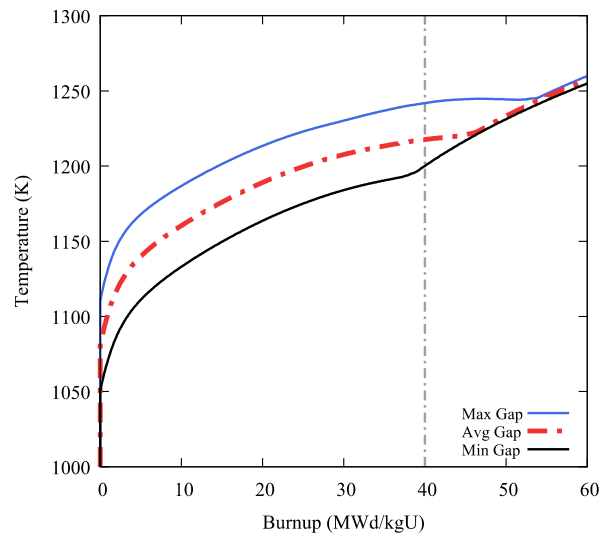
Figure 2. The peak fuel centerline temperatures for the top-mid section of fuel rod 3 show an expected difference based on the variation of the gap thickness among the simulations.

Figure 3 shows the cladding radial expansion and the cladding elongation over the simulated fuel utilization. As indicated in Fig. 3a, the cladding radius initially increases (~14 µm) due to thermal expansion as the cladding is heated to the coolant temperature. After the cladding is heated, it expands slightly (< 2 µm) due to irradiation swelling. As mechanical contact occurs and the edge of the fuel pellet stack pushes on the cladding, the cladding begins to radially deform locally. Shortly after the onset of mechanical interaction has occurred, mechanical contact is fully established between the cladding wall and the fuel stack. As the fuel continues to radially expand, the axial elongation (shown in Figure 3b) due to irradiation swelling is offset. The initially cladding elongation is also due to thermal expansion as the cladding is heated from room temperature to reactor coolant temperature. During constant power operation, the

cladding continues to expand due to isotropic irradiation swelling until mechanical contact is established. Here, the cladding is radially deformed, and the cladding axially contracts.
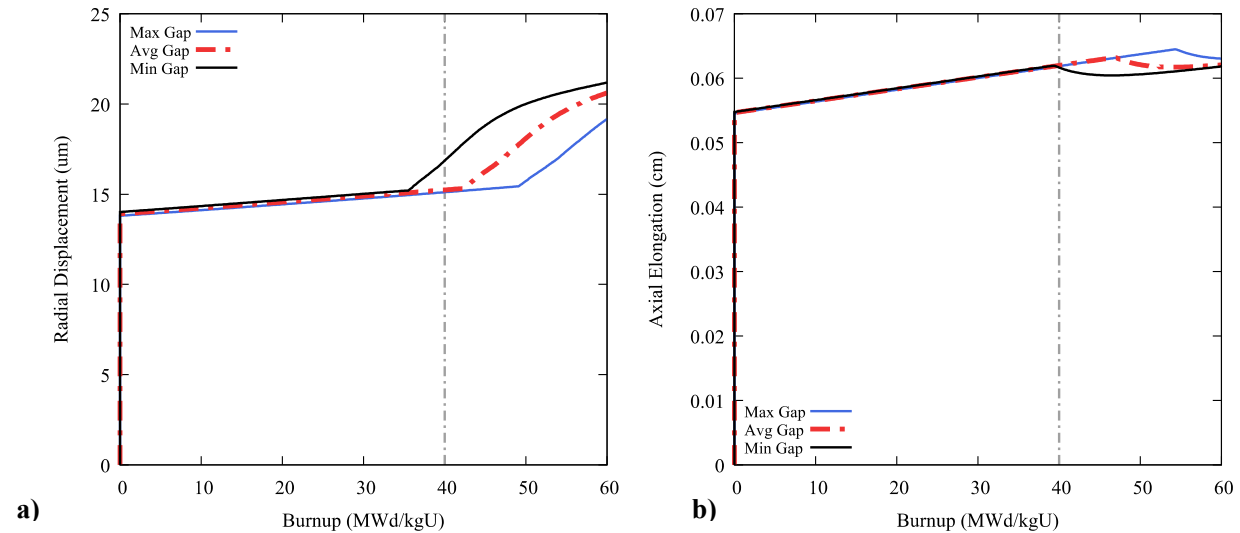
Figure 3. The maximum radial displacement (a) from these simulations is dominated by the initial thermal expansion until mechanical contact with the fuel begins to push the cladding radially. Likewise, axial elongation of the cladding (b) increases initially due to thermal expansion; however, as mechnical contact increases the fuel radial displacment, the elongation is decreased.

The maximum cladding hoop stress over the simulated fuel irradiation, shown in Figure 4, initially becomes compressive due to the large pressure differential between the coolant and fuel rod plenum. There is a slight difference among the hoop stresses in these simulations because of the difference in cladding geometries that results in a different onset burnup for gap closure. There is also a decrease in the hoop stress over time, attributable to the increasing radius due to isotropic irradiation swelling. After gap closure occurs, the hoop stress quickly becomes tensile as the fuel pushes radially on the cladding. Only the minimum gap simulation shows gap closure (~35 MWd/kgU) before the target burnup is reached.
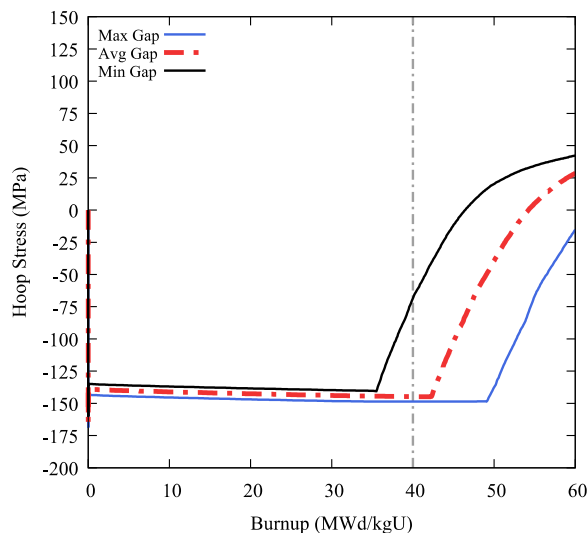
Figure 4. The maximum hoop stress in the cladding is initially compressive due to the pressure difference across the cladding from the coolant system and the fuel rod plenum. It remains compressive until mechanical contact occurs.

Figure 5 shows the calculated results for fission gas release and plenum pressure for rod 3. As indicated in Fig. 5a, a relatively low amount of fission gas is released as expected from the low fuel temperatures (< 1300K). As well, the

modeling predicts that the onset of fission gas release occurs late in the fuel lifetime, at burnup levels near the IFA-796 irradiation target. The low fuel temperatures expected from these fuel rods delays the onset of gas release and also facilitate a smaller amount of fission gas being released to the plenum over the irradiation (< 2% total fission gas production).

As the fuel rod is heated from room temperature to the reactor coolant temperature, the fuel rod plenum pressure (shown in Figure 5b) increases from 1 MPa to ~2.5 MPa. Fuel expansion due to fission product swelling and fuel relocation only increases the plenum pressure slightly up to ~35 MWd/kgU. Even though there is only a small amount of fission gas released to the plenum, there is an increase in pressure near the end of the simulation.
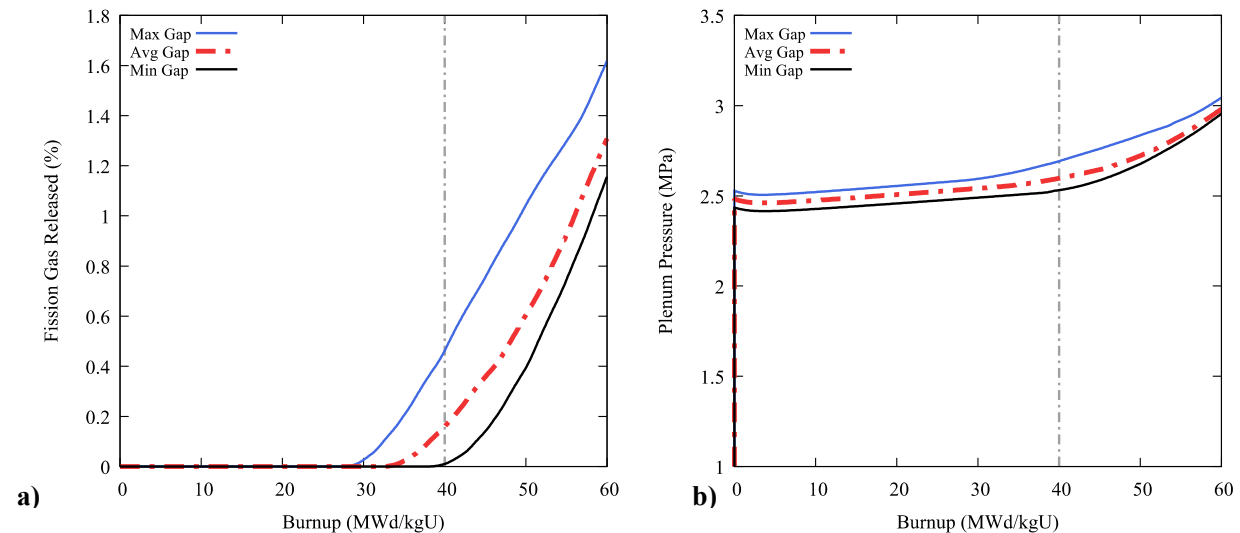
Figure 5. The onset of fission gas release to the fuel rod plenum (a) begins late in the simulation and the amount of gas released remains low (< 1.6%) for all three fuel rod geometries. As there is only a small amount of fission gas released, the fuel rod plenum pressure (b) is only slightly increased starting near the end of the simulations.

The results from these BISON simulations indicate a range of behavior that may be expected during the irradiation of the top-mid section of rod 3 in IFA-796 based on the fuel rod geometry. The *Avg Gap* simulations from the bottom and top-mid sections of fuel rod 3 are compared in order to identify differences in expected integral fuel rod behavior arising from an increase in the coolant temperature profile. For the top-mid section of rod 3, the coolant temperature profile ranges linearly from ~580K to ~587K. In order to simulate the bottom section, the temperature is decreased to 568K to ~574K. Because the temperature difference is so small (~12K), many of the performance aspects examined between the two fuel rod segments are nearly identical.

Figure 6a shows a comparison of the peak fuel centerline temperatures for the *Avg Gap* simulation of the rod 3 segments. The peak fuel centerline temperature for the Top-mid rod segment is consistently 10-15K higher that the temperatures in the Bottom segment. As such, thermally driven phenomena, such as fuel and cladding thermal expansion and fission gas release are slightly decreased. Figure 6b shows the maximum cladding hoop stress and gap closure behavior for these fuel rods is expected to be very similar.
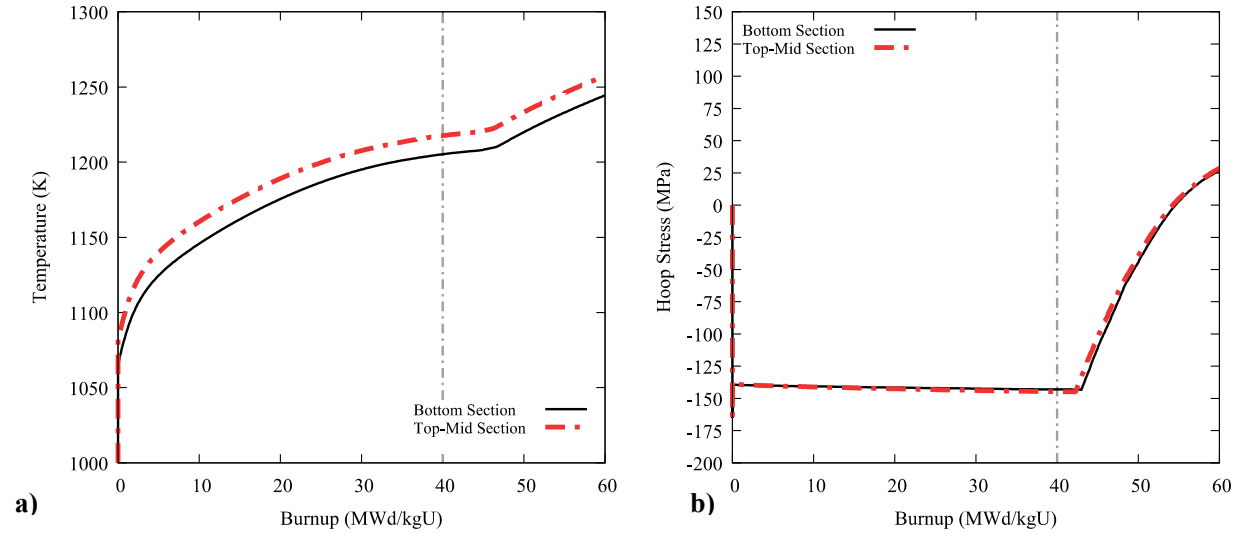
Figure 6. The maximum fuel centerline temperature (a) shows a slight difference between simulations due to the difference in coolant temperatures. The maximum cladding hoop stress (b) for both of the simulations look nearly identical, showing very similar expected mechanical performance for both fuel rod segments.

3.2 Rod 4

IFA-796 rod 4 is a full-length rod (60 cm), spanning 4 sections of the irradiation test rig. Much like the previously discussed results for the segments of rod 3, the fuel temperatures vary based on the fuel rod radial geometry. Initially, the fuel temperatures increase as the fuel power is ramped to 20 kW/m and held constant. Figure 7 shows the peak fuel centerline temperature for each of the Rod 4 simulations. For each successive simulation with a larger initial gap thickness, the fuel temperature is greater. The fuel rod gap behavior dominates the heat transfer between the fuel and the cladding until the gap is closed later in the simulations. During this time, the fuel radius changes due to thermal expansion, densification, fission product swelling, and relocation. Even as the fuel radius is changing however, the thermal conductivity of the fuel is continuously decreasing with increasing fuel utilization. This causes the peak fuel centerline temperature to increase even after gap closure has occurred. Because fuel radial geometry and linear heat rate are the same for rod 4 as the previously discussed rod 3 segments, the fuel centerline temperatures and gap closure times for each of the three simulations is similar.
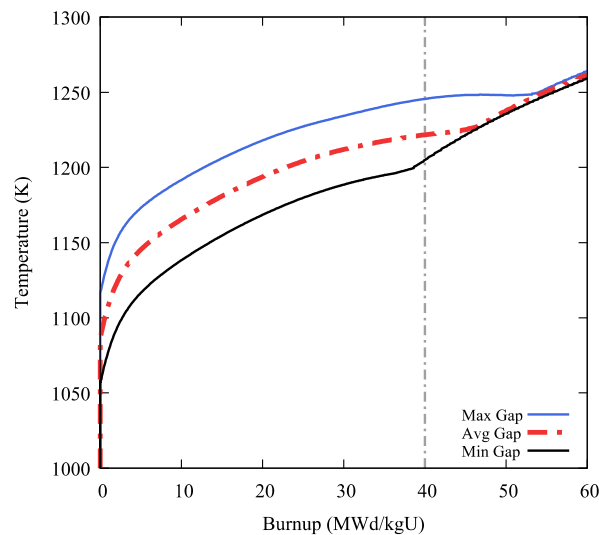

Figure 7. The peak fuel centerline temperature for the rod 4 simulations, as expected, is greater for fuel geometries with correspondingly larger initial gap thicknesses, and shows a very similar progression to the rod 3 simulations.

The maximum cladding radial deformation, shown in Figure 8a, is also very similar to the simulations of rod 3 because of the same radial geometry. The cladding thermally expands as it is heated from room temperature to the coolant temperature. Isotropic irradiation swelling acts to further expand the cladding radius, albeit slowly, until mechanical contact occurs. As marked by the sharp increase in radial displacement, the onset of mechanical contact occurs for the *Min Gap, Avg Gap and Max Gap* simulations at ~35 MWd/kgU, 42 MWd/kgU, and 50 MWd/kgU respectively.

The cladding axial elongation, shown in Figure 8b, displays a similar profile to rod 3, however, because the cladding in rod 4 is longer, the magnitude of the elongation is greater. Again, the initial thermal expansion dominates the cladding axial elongation. The cladding axially expands due to irradiation swelling until mechanical contact occurs. After gap closure is fully established with the full fuel stack pushing on the cladding tube wall, the cladding length will be reduced with increasing radial deformation.
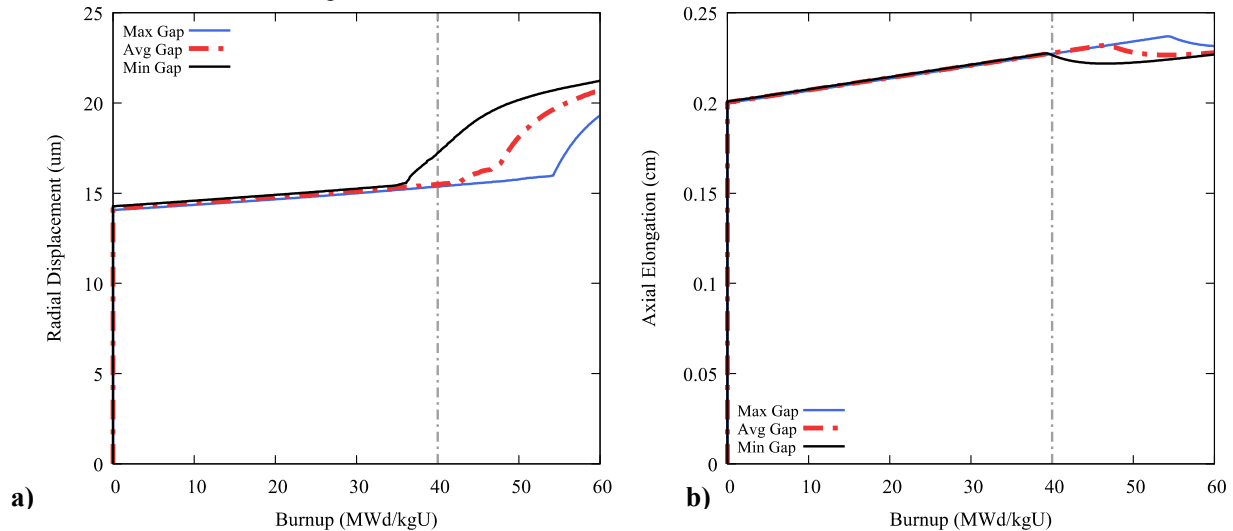
Figure 8. The maximum radial displacement (a) in the cladding initally increases due to thermal expansion. Isotropic irradiation swelling slightly expands the cladding radius until mechanical contact occurs. Thermal expansion is also responsible for the initial cladding elongaiton (b). Similiarly, the cladding expands due to irradiation swelling until mechanical contact occurs and the radial expansion decreases the elongation.

The maximum value of the cladding hoop stress (Fig. 9) initially becomes compressive as the coolant system pressure is much larger than the fuel rod plenum pressure. As reactor operation continues, the cladding hoop stress remains compressive until fuel cladding mechanical contact occurs. After mechanical contact is established, the maximum cladding hoop stress quickly begins to increase, even becoming tensile by 60 MWd/kgU in the *Avg* and *Min Gap* simulations. Of course, much of this behavior is well beyond the 40 MWd/kgU target fuel burnup for this irradiation.
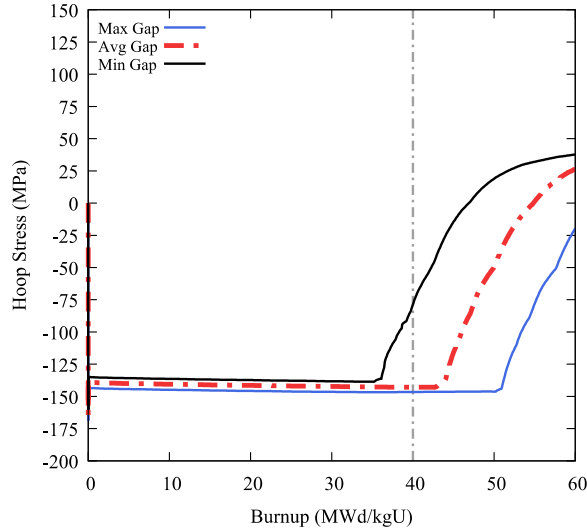
Figure 9. The hoop stress in the cladding initially becomes compressive due to the pressure difference between the fuel rod plenum and the coolant system. After mechanical contact occurs, the hoop stress quickly becomes tensile, and eventually saturates due to the stress sensitivity of the fuel creep model.

The percentage of fission gas released from the fuel is shown in Figure 10a. As indicated in the figure and discussed previously, very little fission gas release is expected in these fuel rods due to the low fuel temperatures. This means fission gas release will have a very small impact on the fuel rod plenum pressure (Fig. 10b) and will not contribute much to gap conductivity degradation. Because of the low fuel temperatures, the onset of fission gas release will also occur late in the fuel life, near the target burnup for IFA-796.

Figure 10b shows the fuel rod plenum pressure over the expected fuel utilization. The plenum pressure increases and the fuel, cladding, and rod fill gas heat to operating temperature. After this, the plenum pressure increases slightly as the plenum volume is decreased from fuel expansion. Starting near 40 MWd/kgU and continuing to the end of the simulation, there is a slight pressure increase from the fission gas released to the plenum.
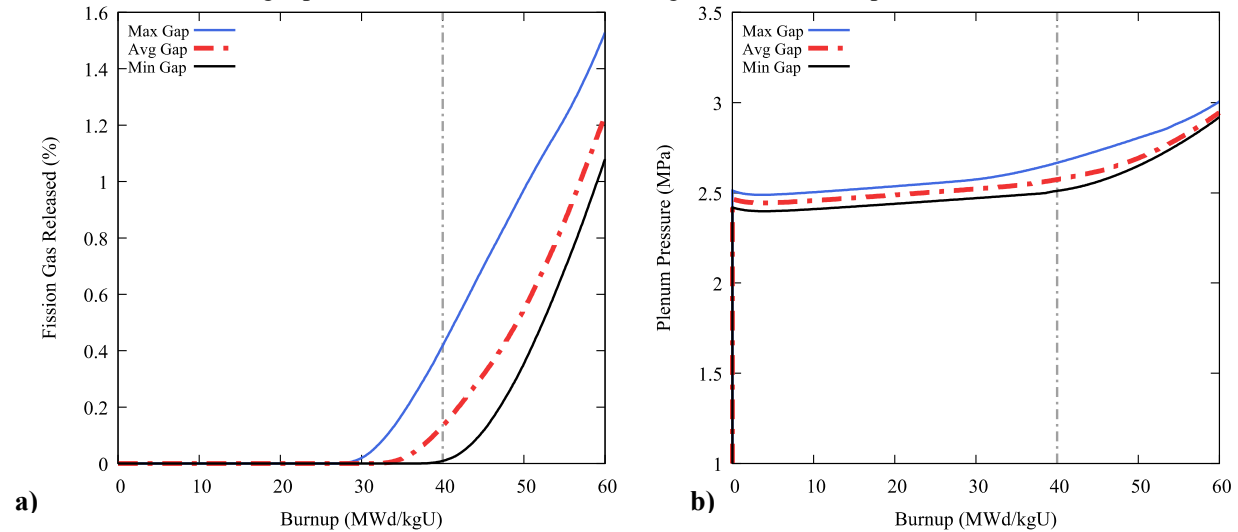
Figure 10. Due to the low (< 1300 K) fuel temperatures, the onset of fission gas release (a) is expected to occur near the IFA-796 target burnup, and the total amount of fission gas released is expected to be less than 1.6%. The fuel rod plenum pressure increases from 1 MPa to ~ 2.5 MPa as the fuel rod is initially heated. Fuel expansion gradually decreases the plenum volume, thereby increasing the plenum pressure, until fission gas is released from the fuel.

3.3 Rod 4 – Fuel Creep Analysis

For this scoping analysis, the performance impact of modifying the fuel creep model on the average gap thickness simulation using rod 4 geometry is identified.

Figure 11 shows the maximum cladding radial displacement (a) and cladding hoop stress (b) for the *Avg Gap* simulation of IFA-796 rod 4, and compares the original fuel creep model and the modified fuel creep model. As mentioned previously, the only difference between these fuel creep models is the contribution of the fission-induced creep term. There is no noticeable change in the cladding behavior before mechanical contact has occurred. There is a slight increase in the radial displacement after the fuel comes into contact with cladding, as the fuel is actually less compliant after modifying the creep model. Using the modified fuel creep models, the fuel deforms less due to mechanical contact, expanding the cladding further than the original model and generating somewhat higher hoop stresses in the cladding. More work is set to be performed to benchmark this model in order to correctly determine cladding behavior after mechanical contact has occurred.
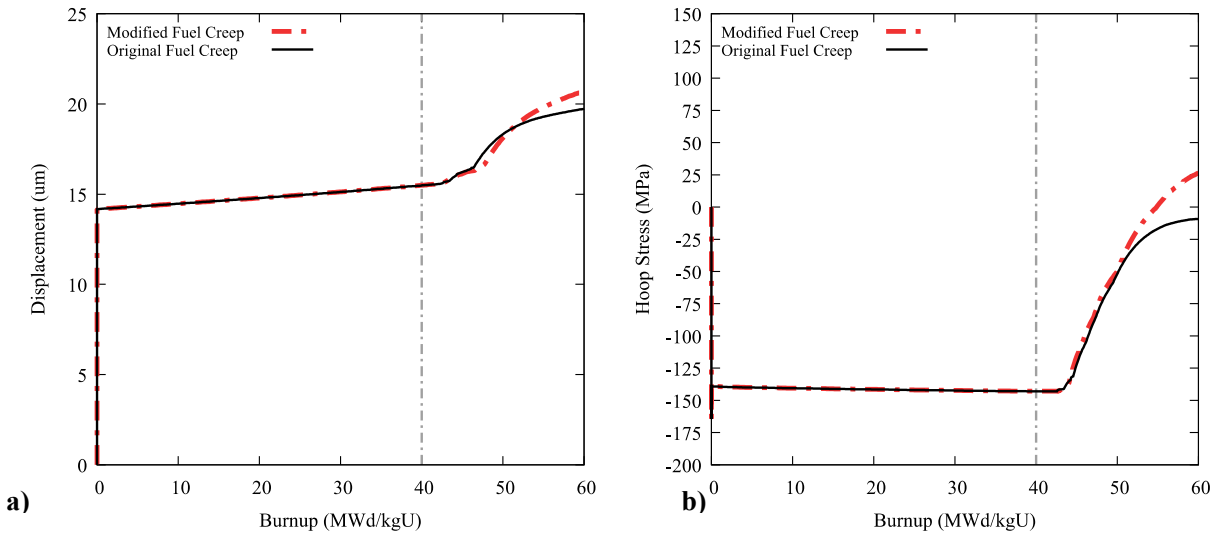

Figure 11. By modifying the fission-induced creep contribution in the fuel, the maximum cladding radial displacement (a) and maximum cladding hoop stress (b) are increased compared to the original fission-induced creep contribution after mechanical contact has occurred at ~ 42 MWd/kgU.

Next, the effect grain size within the fuel creep model was analyzed for rod 4. Because it is currently impractical to track individual grain evolution in a continuum-scale fuel performance code, BISON uses a static value for the grain size in fuel creep calculations. This short analysis applied a simple linear grain size profile to the Rod 4 fuel geometry. To perform this, the fuel is divided into four concentric zones, where each has a different grain diameter. A radial slice from the axisymmetric fuel rod mesh is shown in Figure 15. Starting from the innermost zone and proceeding toward the fuel periphery the grain diameters for each zone are: 10µm, 7.33 µm, 4.66 µm, and 2 µm. The values from this simplified profile are chosen to determine the effect of grain subdivision approaching the periphery of the fuel pellet. Grain growth here is neglected because, according to Ainscough et al., the 10 µm grain size should be very near the limiting grain size for these temperatures [14].
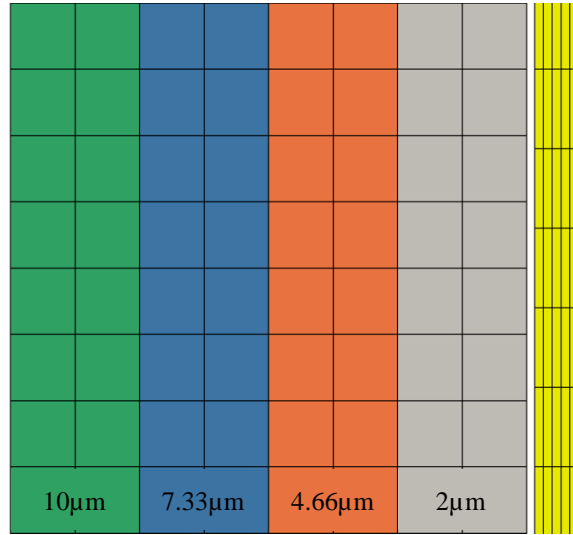
Figure 12. This axial segment of the axisymmetric fuel rod mesh shows the four regions of the UO$_2$ fuel and the FeCrAl cladding which are considered in this analysis. Starting from the center (green) and progressing toward the FeCrAl cladding (yellow) all four fuel zones has a progressively smaller grain size.

The resulting cladding hoop stress profiles for these simulations, shown in Figure 13, show similar results even when including this modification to the fuel geometry. This shows that the magnitude of the fuel creep calculated from modifying the first term in equation 1 (grain boundary sliding and vacancy diffusion) shows little to no effect on the fuel in these particular simulations and the corresponding experimental conditions. This highlights the importance of accurately determining the fission-induced creep contribution, as it dominates the total creep response under these anticipated low fuel temperatures (<1300K).
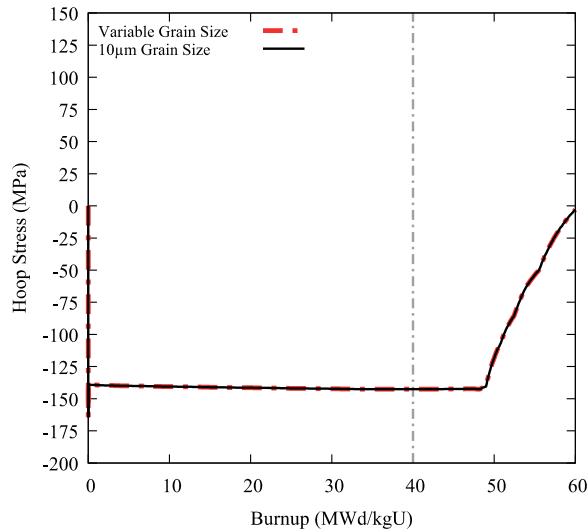
Figure 13. The maximum cladding hoop stress in these simulations remains unaffected by the differing grain sizes. This indicates that nearly the entire creep response is due to the contribution from fission-induced creep.

4.   SUMMARY and CONCLUSIONS

Three FeCrAl cladded fuel rods from IFA-796 were simulated using the BISON fuel performance code. These simulations use models developed from available data on the C35M alloy and expected reactor operating conditions for the PWR test loop used in the experiment. Due to small variations in the fuel diameter and cladding thickness during manufacture, a range of values were used in the fuel rod geometry in these simulations. The analysis performed in Sections 3.1 and 3.2 show that the expected temperature during steady state operation for both rod 3 and rod 4 should   This analysis also shows an almost negligible difference in the performance of the rod 3 segments based on the axial location.

Effects from modifying the fuel creep model were identified for the BISON simulations of the IFA-796 rod 4 experiment, but show that varying the creep model (within the range investigated here) only provide a minimal increase in the fuel radius and maximum cladding hoop stress. Continued investigation of fuel behavioral models will include benchmarking the modified fuel creep model against available experimental data, as well as an investigation of the role that fuel cracking will play in the compliance of the fuel. Correctly calculating stress evolution in the fuel is key to assessing fuel behavior up to gap closure and the subsequent deformation of the cladding due to PCMI. The inclusion of frictional contact should also be investigated to determine the axial elongation of the fuel rods for comparison with data from this experiment.

5. REFERENCES

[1]   Hofmann, P., *J Nucl Mater* **1998,** *270*, 194-211.

[2]   Terrani, K. A., Zinkle, S. J., Snead, L. L., *Journal of Nuclear Materials* **2014,** *448* (1-3), 420-435.

[3]   Williamson, R. L.*, et al.*, *J Nucl Mater* **2012,** *423* (1-3), 149-163.

[4]   Terrani, K. A.*, et al. Characterization Report on FeCrAl Cladding for Halden Irradiation, ORNL/TM-2016/343*; Oak Ridge National Laboratory: July 2016, 2016.

[5]   Gamble, K. A.*, et al.*, *J Nucl Mater* **2017,** *491*, 55-66.

[6]   Thompson, Z. T.*, et al. Elastic Modulus Measurement of ORNL ATF FeCrAl Alloys*; Oak Ridge National Laboratory (ORNL), Oak Ridge, TN (United States): 2015.

[7]   Kanthal, Kanthal APMT Datasheet. Sandvik AB: Hallstahammar, Sweden.

[8]   Terrani, K. A.; Yamamoto, Y. *Input Correlations for Irradiation Creep of FeCrAl and SiC Based on In-Pile Halden Test Results*; Oak Ridge National Laboratory (ORNL), Oak Ridge, TN (United States): 2016.

[9]   Sweet, R. T.*, et al.*, *Nucl Eng Des* **2017**, Manuscript submitted for publication.

[10]   Hales, J.*, et al.*, BISON theory manual: The equations behind nuclear fuel analysis. Fuels Modeling & Simulation Department, Idaho National Laboratory, Idaho Falls, Idaho: 2014.

[11]   Hagrman, D. T.*, et al. SCDAP/RELAP5/MOD 3.1 code manual: MATPRO, A library of materials properties for Light-Water-Reactor accident analysis. Volume 4*; NUREG/CR--6150-Vol.4; EGG--2720-Vol.4;; 1995.

[12]   Solomon, A. A.*, et al. Fission-Induced Creep of UO2 and Its Significance to Fuel-Element Performance.*; ANL-7857; Argonne National Lab., Argonne, Illinois 1971.

[13]   Dienst, W., *J Nucl Mater* **1977,** *65*, 1-8.

[14]   Ainscough, J. B.*, et al.*, *J Nucl Mater* **1973,** *49* (2), 117-128.